

COMBINING THE MIE-LENNARD-JONES AND MODEL ATOMIC POTENTIALS IN STUDYING THE ELASTIC DEFORMATION OF INTERSTITIAL ALLOY FeSi WITH BCC STRUCTURE UNDER PRESSURE

Nguyen Quang Hoc¹, Nguyen Duc Hien², Nguyen Minh Hoa³
and Vu Quoc Trung¹

¹*Faculty of Physics, Hanoi National University of Education*

²*Mac Dinh Chi High School, Gia Lai province*

³*Faculty of Fundamental Sciences, Hue University of Medicine and Pharmacy, Hue University*

Abstract. The mean nearest neighbor distance between two atoms, the Helmholtz free energy and characteristic quantities for elastic deformation such as elastic moduli E , G , K , and elastic constants C_{11} , C_{12} , C_{44} for binary interstitial alloys with BCC structure under pressure are derived from the statistical moment method. The numerical calculations for interstitial alloy FeSi are performed by combining the Mie-Lennard-Jones potential and the model atomic potential. Our calculated results are compared with other calculations and the experimental data.

Keywords: elastic deformation, interstitial alloy, Mie-Lennard-Jones potential, model atomic potential, and statistical moment method.

1. Introduction

Using the statistical moment method (SMM) we have been studied the elastic deformation for body centered cubic (BCC) and face centered cubic (FCC) ternary and binary interstitial alloys under pressure in Ref. [1-10]. In those papers, we always apply the Mie-Lennard-Jones pair potential [11], the Morse pair potential [12] and the Finnis-Sinclair N-body potential [13].

Transition metals such as iron, gold, silver, etc., and their alloys are widely used in structural, electrical, and other technological applications. The dependence of elastic and nonlinear deformations of materials on temperature and pressure has a very important role to predict and understand their interatomic interactions, strength, mechanical stability, phase transition mechanisms, and dynamical response. Iron silicides have paid attention in recent decades due to their unusual physical properties and functional applications. Silicon has been proposed to be a potential light element in the Earth's core based on density, velocity, isotopic and geochemical data [14, 15]. In order to assess Si

Received May 14, 2020. Revised June 15, 2020. Accepted June 22, 2020.

Contact Nguyen Quang Hoc, e-mail address: hocnq@hnue.edu.vn

as a constituent of the core, it is necessary to determine the physical properties of the Si-bearing iron phase under extreme conditions.

We have been considered the structural and thermodynamic properties of BCC-FeSi in the range of temperature from 0 to 1000 K, the range of pressure from 0 to 70 GPa and the range of interstitial atom from 0 to 5% by the way of SMM in Ref. [16-18].

In the present paper, we will present the theory of elastic deformation for binary interstitial alloys with BCC structure at zero pressure and under pressure built by the SMM. Then, we apply this theory to study the elastic deformation of interstitial alloy FeSi by combining the Mie-Lennard-Jones pair potential and the model atomic potential [19]. The SMM calculations through this combination have analogical results as that using only the Mie-Lennard-Jones pair potential and do not apply the process of fitting with the experimental data as in Ref. [28].

2. Content

2.1. Theory of elastic deformation for BCC interstitial alloy AB under pressure

In our model for interstitial alloy AB with BCC structure and concentration condition $c_B \ll c_A$, the cohesive energy u_0 and the alloy parameters $k, \gamma_1, \gamma_2, \gamma$ (k is called as the harmonic parameter and $\gamma_1, \gamma_2, \gamma$ are called as anharmonic parameters) for the interstitial atom B in face centers of the cubic unit cell, the main metal atom A_1 in body center of the cubic unit cell and the main metal atom A_2 in corners of the cubic unit cell in the approximation of two coordination spheres have the form [1-10,16-18, 20]

$$u_{0B} = \frac{1}{2} \sum_{i=1}^{n_i} \varphi_{AB}(r_i) = \varphi_{AB}(r_{1B}) + 2\varphi_{AB}(r_{2B}), \quad r_{2B} = \sqrt{2}r_{1B}, \quad (1)$$

$$k_B = \frac{1}{2} \sum_i \left(\frac{\partial^2 \varphi_{AB}}{\partial u_{i\beta}^2} \right)_{eq} = \frac{1}{r_{1B}} \frac{d\varphi_{AB}(r_{1B})}{dr_{1B}} + \frac{d^2 \varphi_{AB}(r_{2B})}{dr_{2B}^2} + \frac{1}{r_{2B}} \frac{d\varphi_{AB}(r_{2B})}{dr_{2B}}, \quad (2)$$

$$\gamma_B = 4(\gamma_{1B} + \gamma_{2B}), \quad (3)$$

$$\begin{aligned} \gamma_{1B} = \frac{1}{48} \sum_i \left(\frac{\partial^4 \varphi_{AB}}{\partial u_{i\beta}^4} \right)_{eq} &= \frac{1}{24} \frac{1}{8r_{1B}^2} \frac{d^2 \varphi_{AB}(r_{1B})}{dr_{1B}^2} - \frac{1}{8r_{1B}^3} \frac{d\varphi_{AB}(r_{1B})}{dr_{1B}} + \frac{1}{48} \frac{d^4 \varphi_{AB}(r_{2B})}{dr_{2B}^4} + \\ &+ \frac{1}{8r_{2B}} \frac{d^3 \varphi_{AB}(r_{2B})}{dr_{2B}^3} - \frac{5}{16r_{2B}^2} \frac{d^2 \varphi_{AB}(r_{2B})}{dr_{2B}^2} + \frac{5}{16r_{2B}^3} \frac{d\varphi_{AB}(r_{2B})}{dr_{2B}}, \end{aligned} \quad (4)$$

$$\begin{aligned} \gamma_{2B} = \frac{6}{48} \sum_i \left(\frac{\partial^4 \varphi_{AB}}{\partial u_{i\alpha}^2 \partial u_{i\beta}^2} \right)_{eq} &= \frac{1}{4r_{1B}^2} \frac{d^2 \varphi_{AB}(r_{1B})}{dr_{1B}^2} - \frac{1}{4r_{1B}^3} \frac{d\varphi_{AB}(r_{1B})}{dr_{1B}} + \frac{1}{8} \frac{d^4 \varphi_{AB}(r_{2B})}{dr_{2B}^4} + \\ &+ \frac{1}{4r_{2B}} \frac{d^3 \varphi_{AB}(r_{2B})}{dr_{2B}^3} + \frac{7}{8r_{2B}^2} \frac{d^2 \varphi_{AB}(r_{2B})}{dr_{2B}^2} - \frac{7}{8r_{2B}^3} \frac{d\varphi_{AB}(r_{2B})}{dr_{2B}}, \end{aligned} \quad (5)$$

$$u_{0A_1} = u_{0A} + \varphi_{AB}(r_{1A_1}), \quad (6)$$

Combining the Mie-Lennard-Jones and model atomic potentials in studying the elastic...

$$k_{A_1} = k_A + \frac{1}{2} \sum_i \left[\left(\frac{\partial^2 \varphi_{AB}}{\partial u_{i\beta}^2} \right)_{\text{eq}} \right]_{r=r_{1A_1}} = k_A + \frac{d^2 \varphi_{AB}(r_{1A_1})}{dr_{1A_1}^2} + \frac{2}{r_{1A_1}} \frac{d\varphi_{AB}(r_{1A_1})}{dr_{1A_1}}, \quad (7)$$

$$\gamma_{A_1} = 4(\gamma_{1A_1} + \gamma_{2A_1}), \quad (8)$$

$$\gamma_{1A_1} = \gamma_{1A} + \frac{1}{48} \sum_i \left[\left(\frac{\partial^4 \varphi_{AB}}{\partial u_{i\beta}^4} \right)_{\text{eq}} \right]_{r=r_{1A_1}} = \gamma_{1A} + \frac{1}{24} \frac{d^4 \varphi_{AB}(r_{1A_1})}{dr_{1A_1}^4} + \frac{1}{4r_{1A_1}^2} \frac{d^2 \varphi_{AB}(r_{1A_1})}{dr_{1A_1}^2} - \frac{1}{4r_{1A_1}^3} \frac{d\varphi_{AB}(r_{1A_1})}{dr_{1A_1}}, \quad (9)$$

$$\gamma_{2A_1} = \gamma_{2A} + \frac{6}{48} \sum_i \left[\left(\frac{\partial^4 \varphi_{AB}}{\partial u_{i\alpha}^2 \partial u_{i\beta}^2} \right)_{\text{eq}} \right]_{r=r_{1A_1}} = \gamma_{2A} + \frac{1}{2r_{1A_1}} \frac{d^3 \varphi_{AB}(r_{1A_1})}{dr_{1A_1}^3} - \frac{3}{4r_{1A_1}^2} \frac{d^2 \varphi_{AB}(r_{1A_1})}{dr_{1A_1}^2} + \frac{3}{4r_{1A_1}^3} \frac{d\varphi_{AB}(r_{1A_1})}{dr_{1A_1}}, \quad (10)$$

$$u_{0A_2} = u_{0A} + \varphi_{AB}(r_{1A_2}), \quad (11)$$

$$k_{A_2} = k_A + \frac{1}{2} \sum_i \left[\left(\frac{\partial^2 \varphi_{AB}}{\partial u_{i\beta}^2} \right)_{\text{eq}} \right]_{r=r_{1A_2}} = k_A + 2 \frac{d^2 \varphi_{AB}(r_{1A_2})}{dr_{1A_2}^2} + \frac{4}{r_{1A_2}} \frac{d\varphi_{AB}(r_{1A_2})}{dr_{1A_2}}, \quad (12)$$

$$\gamma_{A_2} = 4(\gamma_{1A_2} + \gamma_{2A_2}), \quad (13)$$

$$\gamma_{1A_2} = \gamma_{1A} + \frac{1}{48} \sum_i \left[\left(\frac{\partial^4 \varphi_{AB}}{\partial u_{i\beta}^4} \right)_{\text{eq}} \right]_{r=r_{1A_2}} = \gamma_{1A} + \frac{1}{24} \frac{d^4 \varphi_{AB}(r_{1A_2})}{dr_{1A_2}^4} + \frac{1}{4r_{1A_2}} \frac{d^3 \varphi_{AB}(r_{1A_2})}{dr_{1A_2}^3} - \frac{1}{8r_{1A_2}^2} \frac{d^2 \varphi_{AB}(r_{1A_2})}{dr_{1A_2}^2} + \frac{1}{8r_{1A_2}^3} \frac{d\varphi_{AB}(r_{1A_2})}{dr_{1A_2}}, \quad (14)$$

$$\gamma_{2A_2} = \gamma_{2A} + \frac{6}{48} \sum_i \left[\left(\frac{\partial^4 \varphi_{AB}}{\partial u_{i\alpha}^2 \partial u_{i\beta}^2} \right)_{\text{eq}} \right]_{r=r_{1A_2}} = \gamma_{2A} + \frac{1}{4} \frac{d^4 \varphi_{AB}(r_{1A_2})}{dr_{1A_2}^4} - \frac{1}{4r_{1A_2}} \frac{d^3 \varphi_{AB}(r_{1A_2})}{dr_{1A_2}^3} + \frac{3}{2r_{1A_2}^2} \frac{d^2 \varphi_{AB}(r_{1A_2})}{dr_{1A_2}^2} - \frac{3}{2r_{1A_2}^3} \frac{d\varphi_{AB}(r_{1A_2})}{dr_{1A_2}}, \quad (15)$$

where φ_{AB} is the interaction potential between atoms A and B, $r_{1X} = r_{01X} + y_{0X}(T)$ is the nearest neighbor distance between the atom X ($X = A, A_1, A_2, B$) (A in clean metal, A_1, A_2 and B in interstitial alloy AB) and other atoms at temperature T, r_{01X} is the nearest neighbor distance between the atom X and other atoms at $T = 0$ K and is determined from the minimum condition of the cohesive energy $u_{0X}, y_{0X}(T)$ is the displacement of atom X from equilibrium position at temperature T. $u_{0A}, k_A, \gamma_{1A}, \gamma_{2A}$ are the corresponding quantities in the clean metal A with BCC structure in the approximation of two coordination spheres [20]

$$u_{0A} = 4\varphi_{AA}(r_{1A}) + 3\varphi_{AA}(r_{2A}), \quad r_{2A} = \frac{2}{\sqrt{3}} r_{1A}, \quad (16)$$

$$k_A = \frac{4}{3} \frac{d^2\varphi_{AA}(r_{1A})}{dr_{1A}^2} + \frac{8}{3r_{1A}} \frac{d\varphi_{AA}(r_{1A})}{dr_{1A}} + \frac{d^2\varphi_{AA}(r_{2A})}{dr_{2A}^2} + \frac{2}{r_{2A}} \frac{d\varphi_{AA}(r_{2A})}{dr_{2A}}, \quad (17)$$

$$\begin{aligned} \gamma_{1A} = & \frac{1}{54} \frac{d^4\varphi_{AA}(r_{1A})}{dr_{1A}^4} + \frac{8}{9r_{1A}} \frac{d^3\varphi_{AA}(r_{1A})}{dr_{1A}^3} - \frac{20}{9r_{1A}^2} \frac{d^2\varphi_{AA}(r_{1A})}{dr_{1A}^2} + \frac{20}{9r_{1A}^3} \frac{d\varphi_{AA}(r_{1A})}{dr_{1A}} + \\ & + \frac{1}{24} \frac{d^4\varphi_{AA}(r_{2A})}{dr_{2A}^4} + \frac{1}{4r_{2A}^2} \frac{d^2\varphi_{AA}(r_{2A})}{dr_{2A}^2} - \frac{1}{4r_{2A}^3} \frac{d\varphi_{AA}(r_{2A})}{dr_{2A}}, \end{aligned} \quad (18)$$

$$\begin{aligned} \gamma_{2A} = & \frac{1}{54} \frac{d^4\varphi_{AA}(r_{1A})}{dr_{1A}^4} + \frac{5}{9r_{1A}} \frac{d^3\varphi_{AA}(r_{1A})}{dr_{1A}^3} + \frac{5}{18r_{1A}^2} \frac{d^2\varphi_{AA}(r_{1A})}{dr_{1A}^2} - \frac{5}{18r_{1A}^3} \frac{d\varphi_{AA}(r_{1A})}{dr_{1A}} + \\ & + \frac{1}{2r_{2A}} \frac{d^3\varphi_{AA}(r_{2A})}{dr_{2A}^3} - \frac{9}{8r_{2A}^2} \frac{d^2\varphi_{AA}(r_{2A})}{dr_{2A}^2} + \frac{9}{8r_{2A}^3} \frac{d\varphi_{AA}(r_{2A})}{dr_{2A}}. \end{aligned} \quad (19)$$

The equations of state for BCC interstitial alloy at temperature T and pressure P and at 0 K and pressure P are written in the form [20]

$$Pv = -r_1 \left(\frac{1}{6} \frac{\partial u_0}{\partial r_1} + \theta x \coth x \frac{1}{2k} \frac{\partial k}{\partial r_1} \right), v = \frac{4r_1^3}{3\sqrt{3}}. \quad (20)$$

$$Pv = -r_1 \left(\frac{1}{6} \frac{\partial u_0}{\partial r_1} + \frac{\hbar\omega_0}{4k} \frac{\partial k}{\partial r_1} \right). \quad (21)$$

From that, we can calculate the nearest neighbor distance $r_{1X}(P,0)$ ($X = A, A_1, A_2, B$), the parameters $k_X(P,0), \gamma_{1X}(P,0), \gamma_{2X}(P,0), \gamma_X(P,0)$, the displacement $y_{0X}(P, T)$ of atom X from equilibrium position as in [20], the nearest neighbor distance $r_{1X}(P, T)$ and the mean nearest neighbor distance between two atoms in alloy $\overline{r_{1A}}(P, T)$ as follows [1-10]:

$$\begin{aligned} r_{1B}(P, T) &= r_{1B}(P, 0) + y_{A_1}(P, T), r_{1A}(P, T) = r_{1A}(P, 0) + y_A(P, T), \\ r_{1A_1}(P, T) &\approx r_{1B}(P, T), r_{1A_2}(P, T) = r_{1A_2}(P, 0) + y_B(P, T). \end{aligned} \quad (22)$$

$$\overline{r_{1A}}(P, T) = \overline{r_{1A}}(P, 0) + \overline{y}(P, T),$$

$$\overline{r_{1A}}(P, 0) = (1 - c_B)r_{1A}(P, 0) + c_B r'_{1A}(P, 0), r'_{1A}(P, 0) = \sqrt{3}r_{1B}(P, 0),$$

$$\overline{y}(P, T) = (1 - 7c_B)y_A(P, T) + c_B y_B(P, T) + 2c_B y_{A_1}(P, T) + 4c_B y_{A_2}(P, T), \quad (23)$$

The Helmholtz free energy of BCC interstitial alloy AB with the condition $c_B \ll c_A$ is determined by Ref. [1-10,15]

$$\begin{aligned} \psi_{AB} &= (1 - 7c_B)\psi_A + c_B\psi_B + 2c_B\psi_{A_1} + 4c_B\psi_{A_2} - TS_c, \\ \psi_X &\approx U_{0X} + \psi_{0X} + 3N \left\{ \frac{\theta^2}{(k_X)^2} \left[\gamma_{2X}(Y_X)^2 - \frac{2\gamma_{1X}}{3} \left(1 + \frac{Y_X}{2} \right) \right] + \right. \\ &+ \left. \frac{2\theta^3}{(k_X)^4} \left[\frac{4}{3} \gamma_{2X} Y_X \left(1 + \frac{Y_X}{2} \right) - 2 \left[(\gamma_{1X})^2 + 2\gamma_{1X}\gamma_{2X} \right] \left(1 + \frac{Y_X}{2} \right) \left(1 + Y_X \right) \right] \right\}, \\ \psi_{0X} &= 3N\theta \left[x_X + \ln(1 - e^{-2x_X}) \right], Y_X \equiv x_X \coth x_X, \end{aligned} \quad (24)$$

where ψ_X is the Helmholtz free energy of one atom X, U_{0X} is the cohesive energy and S_c is the configurational entropy of BCC interstitial alloy AB.

The Young modulus E, the bulk modulus K, the shearing modulus G, the elastic constants C_{11} , C_{12} , C_{44} and the Poisson ratio of BCC interstitial alloy AB have the form [1, 2, 5, 7]

$$E_{AB} = \frac{1}{\pi r_{1A} A_{1A}} \left(1 - 7c_B + c_B \frac{\frac{\partial^2 \psi_B}{\partial \epsilon^2} + 2 \frac{\partial^2 \psi_{A_1}}{\partial \epsilon^2} + 4 \frac{\partial^2 \psi_{A_2}}{\partial \epsilon^2}}{\frac{\partial^2 \psi_A}{\partial \epsilon^2}} \right),$$

$$A_{1A} = \frac{1}{k_A} \left[1 + \frac{2\gamma_A^2 \theta^2}{k_A^4} \left(1 + \frac{Y_A}{2} \right) (1 + Y_A) \right],$$

$$\frac{\partial^2 \psi_X}{\partial \epsilon^2} = \left\{ \frac{1}{2} \frac{\partial^2 u_{0X}}{\partial r_{1X}^2} + \frac{3}{4} \frac{\hbar \omega_X}{k_X} \left[\frac{\partial^2 k_X}{\partial r_{1X}^2} - \frac{1}{2k_X} \left(\frac{\partial k_X}{\partial r_{1X}} \right)^2 \right] \right\} 4r_{01X}^2 +$$

$$+ \left(\frac{1}{2} \frac{\partial u_{0X}}{\partial r_{1X}} + \frac{3}{2} \hbar \omega_X \coth x_X \frac{\partial k_X}{\partial r_{1X}} \right) 2r_{01X}, \quad x_X = \frac{\hbar \omega_X}{2\theta}, \quad \omega_X = \sqrt{\frac{k_X}{m}}, \quad (25)$$

$$K_{AB} = \frac{E_{AB}}{3(1-2\nu_A)}, \quad G_{AB} = \frac{E_{AB}}{2(1+\nu_A)},$$

$$G_{AB} = \frac{E_{AB}}{2(1+\nu_A)}, \quad C_{11AB} = \frac{E_{AB}(1-\nu_A)}{(1+\nu_A)(1-2\nu_A)}, \quad C_{44AB} = \frac{E_{AB}}{2(1+\nu_A)}, \quad (26)$$

$$\nu_{AB} = c_A \nu_A + c_B \nu_B \approx \nu_A, \quad (27)$$

where ν_A, ν_B are the Poisson ratios of materials A and B determined from experiments and because of considering $c_B \approx 0$.

2.2. Numerical results for alloy FeSi

To describe the interactions Fe-Fe and Si-Si, we apply the Mie-Lennard-Jones pair interaction potential in the form [11]

$$\varphi(r) = \frac{D}{n-m} \left[m \left(\frac{r_0}{r} \right)^n - n \left(\frac{r_0}{r} \right)^m \right], \quad (28)$$

where D is the depth of potential well corresponding to the equilibrium distance r_0 , m and n are determined empirically. The Mie-Lennard-Jones potential parameters for the interactions Fe-Fe, Si-Si are given in Table 1. The Poisson ratio of Fe is 0.29 [22].

Table 1. Mie-Lennard-Jones potential parameters for interactions Fe-Fe, Si-Si

Interaction	D (eV)	r_0 (10^{-10} m)	m	n
Fe-Fe [11]	0.401	2.4775	7	11.5
Si-Si [21]	2.32	2.351	2.48	4.0

For the interaction Fe-Si, we still use the model atomic potential as follows [19]

$$\varphi(r) = b_1(r - b_2)^3 + b_3r + b_4 \quad (29)$$

where the parameters b_1, b_2, b_3, b_4 are given in Table 2.

Table 2. Model atomic potential parameters for interaction Fe-Si

Interaction	b_1	b_2	b_3	b_4
Fe – Si[19]	-1.9199	2.8252	0.4445	-2.1427

when $c_{Si} = 0$, we obtain numerical results for Fe as shown in Table 3-10 and Figures 1-3. Our calculated results are summarized in Tables 3-10 and shown in Figures 1-6.

For FeSi at zero pressure and at the same temperature when the concentration of interstitial atoms increases, the mean nearest neighbor distance also increases. For FeSi at zero pressure and in the same concentration of interstitial atoms when temperature increases, the mean nearest neighbor distance also increases (see Table 3 and Table 4). That agrees with the experimental data in [23]. The relative error between the SMM calculations and experiments [23, 24] for the nearest neighbor distance and the volume ratio V/V_0 in different temperatures and pressures are only some percent (see Tables 3 and 4, Figures 1 and 2).

Table 3. The dependence of nearest neighbor distance a_{Fe} (Å) on temperature for Fe at $P = 0$ calculated by the SMM and from experiments (EXPT) [23]

T (K)	293	513	722	822	921	1026	1175	1189
SMM	2.4353	2.4440	2.4529	2.4574	2.4620	2.4670	2.4747	2.4754
EXPT[23]	2.4772	2.4848	2.4925	2.4963	2.5001	2.5043	2.5097	2.5101
$\delta_{SMM-EXPT}$ (%)	1.7	1.6	1.6	1.6	1.5	1.5	1.4	1.4

($\delta_{SMM-EXPT}$ is the relative error between the SMM calculations and experiments)

Table 4. The dependence of volume ratio V/V_0 on pressure for Fe calculated by the SMM and from EXPT[24]

P (GPa)	0	5	10	15	20	25	30
SMM	1	0.990	0.976	0.963	0.952	0.941	0.932
EXPT[24]	1	0.974	0.952	0.932	0.914	0.896	0.879
$\delta_{SMM-EXPT}$ (%)	0	1.6	2.5	3.3	4.2	5.0	6.0

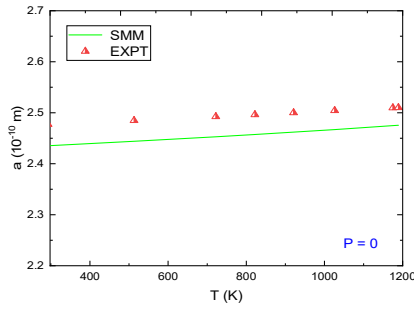


Figure 1. $a(T)$ for Fe at $P = 0$ calculated by the SMM and from EXPT [23]

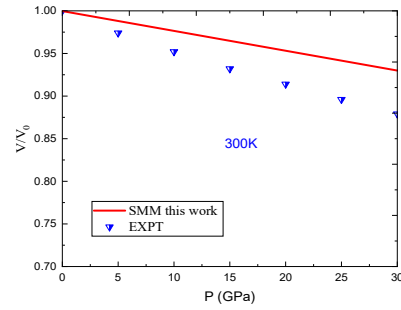


Figure 2. $V/V_0(P)$ for Fe at $T = 300$ K calculated by the SMM and from EXPT [24]

Numerical results for FeSi are summarized in tables from Table 5 to Table 11 and illustrated in Figures 3-9.

Table 5. The mean nearest neighbor distance a_{FeSi} (\AA) for BCC-FeSi at $P = 0$ calculated by the SMM

T (K)	$c_{Si}(\%)$	0	1	2	3	4	5
100	$a_{FeSi}(\text{\AA})$	2.4227	2.4328	2.4429	2.4530	2.4631	2.4732
300		2.4298	2.4401	2.4504	2.4607	2.4710	2.4812
500		2.4374	2.4479	2.4584	2.4689	2.4795	2.4900
700		2.4454	2.4563	2.4671	2.4779	2.4888	2.4996
900		2.4540	2.4655	2.4769	2.4883	2.4998	2.5112
1100		2.4631	2.4760	2.4888	2.5017	2.5145	2.5273
1300		2.4732	2.4889	2.5047	2.5204	2.5361	2.5519
1500		2.4848	2.5057	2.5266	2.5475	2.5684	2.5893

Table 6. The dependence of elastic moduli E , G , K (10^{10} Pa) on temperature and concentration of interstitial atoms for BCC-FeSi at $P = 0$ calculated by the SMM

T (K)	$c_{Si}(\%)$	0	1	2	3	4	5
100	E	22.4667	19.8430	17.4835	14.3640	13.4626	11.7590
	K	17.8307	15.7484	13.8758	12.1937	10.6846	9.3326
	G	8.7080	7.6911	6.7765	5.9550	5.2181	4.5578
300	E	20.8182	18.3150	16.0625	14.0372	12.2180	10.5854
	K	16.5224	14.5357	12.7480	11.1406	9.6968	8.4011
	G	8.0691	7.0988	6.2258	5.4408	4.7357	4.1029
500	E	18.7777	16.3727	14.2057	12.2547	10.5003	8.9253
	K	14.9030	12.9942	11.2744	9.7260	8.3336	7.0835
	G	7.2782	6.3460	5.5061	4.7499	4.0699	3.4594

700	E	16.3755	14.0527	11.9634	10.0889	8.4138	6.9254
	K	12.9965	11.1530	9.4947	8.0071	6.6776	5.4964
	G	6.3471	5.4468	4.6370	3.9104	3.2612	2.6843
900	E	13.6971	11.4443	9.4415	7.6750	6.1331	4.8061
	K	10.8707	9.0827	7.4933	6.0912	4.8676	3.8144
	G	5.3090	4.4358	3.6595	2.9748	2.3772	1.8628
1100	E	10.8992	8.6848	6.7802	5.1714	3.8428	2.7748
	K	8.6502	6.8927	5.3811	4.1043	3.0498	2.2022
	G	4.2245	3.3662	2.6280	2.0044	1.4895	1.0754
1300	E	8.1719	5.9600	4.1943	2.8376	1.8398	1.1402
	K	6.4856	4.7302	3.3288	2.2521	1.4602	0.9050
	G	3.1674	2.3101	1.6257	1.0999	0.7131	0.4420
1500	E	5.6839	3.5224	2.0408	1.1001	0.5493	0.2523
	K	4.5110	2.7955	1.6197	0.8731	0.4359	0.2003
	G	2.2030	1.3653	0.7910	0.4264	0.2129	0.0978

Table 7. The dependence of elastic constants C_{11} , C_{12} , C_{44} (10^{10} Pa) on temperature and concentration of interstitial atoms for BCC-FeSi at $P = 0$ calculated by the SMM

T(K)	$c_{Si}(\%)$	0	1	2	3	4	5
100	C_{11}	29.4414	26.0031	22.9111	20.1337	17.6420	15.4096
	C_{12}	12.0253	10.6210	9.3581	8.2236	7.2059	6.2941
	C_{44}	8.7080	7.6911	6.7765	5.9550	5.2181	4.5578
300K	C_{11}	27.2811	24.0008	21.0490	18.3950	16.0110	13.8716
	C_{12}	11.1430	9.8031	8.5975	7.5135	6.5397	5.6659
	C_{44}	8.0691	7.0988	6.2258	5.4408	4.7357	4.1029
500K	C_{11}	24.6072	21.4556	18.6158	16.0592	13.7601	11.6961
	C_{12}	10.0508	8.7635	7.6036	6.5594	5.6203	4.7773
	C_{44}	7.2782	6.3460	5.5061	4.7499	4.0699	3.4594
700K	C_{11}	21.4593	18.4154	15.6774	13.2210	11.0259	9.0754
	C_{12}	8.7651	7.5218	6.4034	5.4001	4.5035	3.7068
	C_{44}	6.3471	5.4468	4.6370	3.9104	3.2612	2.6843
900K	C_{11}	17.9493	14.9971	12.3726	10.0576	8.0371	6.2982
	C_{12}	7.3314	6.1256	5.0536	4.1080	3.2828	2.5725
	C_{44}	5.3090	4.4358	3.6595	2.9748	2.3772	1.8628
1100K	C_{11}	14.2829	11.3810	8.8851	6.7769	5.0357	3.6362

	C ₁₂	5.8338	4.6487	3.6291	2.7680	2.0569	1.4852
	C ₄₄	4.2245	3.3662	2.6280	2.0044	1.4895	1.0755
1300K	C ₁₁	10.7089	7.8103	5.4965	3.7186	2.4110	1.4942
	C ₁₂	4.3740	3.1901	2.2450	1.5188	0.9848	0.6103
	C ₄₄	3.1674	2.3101	1.6257	1.0999	0.7131	0.4420
1500K	C ₁₁	7.4484	4.6158	2.6743	1.4416	0.7198	0.3307
	C ₁₂	3.0423	1.8854	1.0923	0.5889	0.2940	0.1351
	C ₄₄	2.2030	1.3653	0.7909	0.4264	0.2129	0.0978

According to Tables 4-6, Figures 3 and 4 for FeSi at zero pressure and in the same concentration of interstitial atoms when temperature increases, quantities E, G, K, C₁₁, C₁₂, C₄₄ decrease. For FeSi at zero pressure and in the same temperature when the concentration of interstitial atoms increases, quantities E, G, K, C₁₁, C₁₂, C₄₄ also decrease. We use the Voigt-Reuss-Hill conversion rule [25] for polycrystalline samples as follows:

$$E = \frac{9KG}{3K + G}, K = \frac{C_{11}^* + 2C_{12}^*}{3}, G = \frac{3(C_{11}^* - C_{12}^*)^2 + 38(C_{11}^* - C_{12}^*)C_{44}^* + 12C_{44}^{*2}}{30(C_{11}^* - C_{12}^*) + 40C_{44}^*}. \quad (30)$$

Note: the signal * is used to show elastic quantities of monocrystalline material.

Table 8. The dependence of elastic modulus E (10¹⁰ Pa) on temperature and concentration of interstitial atoms for BCC-FeSi at P = 0 calculated by the SMM, LMTO-GGA [26] and EXPT[27]

T (K)	c _{si} = 0			c _{si} = 1%	c _{si} = 2%
	SMM	LMTO GGA[26]	EXPT[27]		
20	23.03	26.90	22.09	20.36	17.95
60	22.75	26.69	22.05	20.10	17.73
100	22.47	26.49	21.93	19.84	17.48
140	22.17	26.28	21.77	19.59	17.26
180	21.86	26.07	21.63	19.30	17.00
220	21.53	25.87	21.44	19.00	16.73
260	21.18	25.66	21.23	18.68	16.43
300	20.82	25.45	21.01	18.32	16.06
340	20.44	25.24	20.78	17.99	15.79
380	20.05	25.02	20.54	17.62	15.44
420	19.64	24.81	20.30	17.24	15.07
460	19.22	24.60	20.04	16.84	14.69
500	18.78	24.38	19.78	16.37	14.21

(LMTO: Linear Muffin-Tin Orbital)

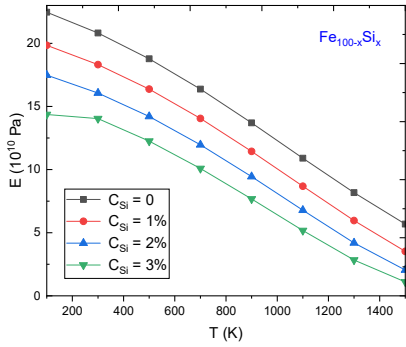


Figure 3. $E(T, c_{Si})(10^{10} \text{ Pa})$ for BCC-FeSi at $P = 0$ calculated by the SMM

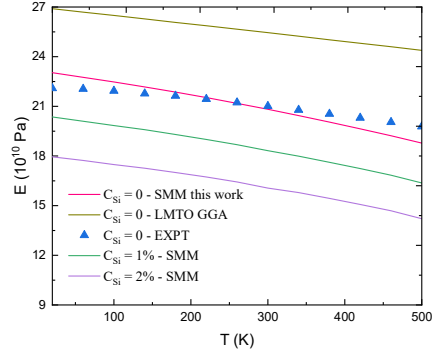


Figure 4. $E(T, c_{Si})(10^{10} \text{ Pa})$ for BCC-FeSi at $P = 0$ calculated by the SMM, LMTO-GGA [26] and EXPT[27]

Table 9. The dependence of mean nearest neighbor distance a_{FeSi} (Å) on pressure and concentration of interstitial atoms for BCC-FeSi at $T = 300\text{K}$ calculated by the SMM

P (GPa)	c_{Si} (%)	0	1	2	3	4	5
10	a_{FeSi} (Å)	2.4102	2.4177	2.4251	2.4326	2.4400	2.4474
20		2.3901	2.3964	2.4027	2.4089	2.4152	2.4215
30		2.3733	2.3788	2.3843	2.3897	2.3952	2.4007
40		2.3588	2.3637	2.3685	2.3734	2.3783	2.3831
50		10.1052	2.3504	2.3548	2.3591	2.3635	2.3678
60		2.3347	2.3386	2.3425	2.3464	2.3503	2.3543
70		2.3243	2.3279	2.3315	2.3350	2.3385	2.3420

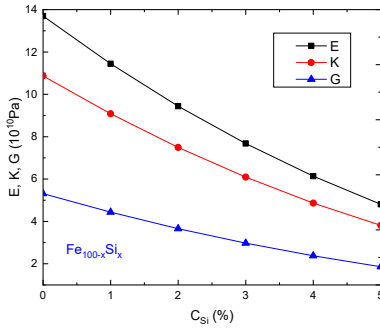


Figure 5. $E, K, G(c_{Si})(10^{10} \text{ Pa})$ for BCC-FeSi at $P = 0, T = 900 \text{ K}$ calculated by the SMM

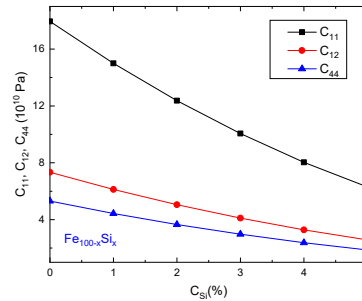


Figure 6. $C_{11}, C_{12}, C_{44}(c_{Si})(10^{10} \text{ Pa})$ for BCC-FeSi at $P = 0, T = 900 \text{ K}$ calculated by the SMM

For the Young modulus of Fe at zero pressure and temperatures $T \leq 500 \text{ K}$, the SMM calculations in this paper are better than calculations in [26] in the comparison with the experimental data in [27] (see Table 7 and Figure 4). Figures 3, 5 and 6 show the dependencies of quantities $E, G, K, C_{11}, C_{12}, C_{44}$ on temperature, and concentration of interstitial atoms for FeSi at zero pressure and $T = 900 \text{ K}$.

Table 10. The dependence of elastic moduli E , G , K (10^{10} Pa) on pressure and concentration of interstitial atoms for BCC-FeSi at $T = 300$ K calculated by the SMM

P (GPa)	csi(%)	0	1	2	3	4	5
10	E	24.6588	22.3584	20.2351	18.2768	16.4720	14.8099
	K	19.5705	17.7447	16.0596	14.5054	13.0730	11.7539
	G	9.5577	8.6660	7.8431	7.0840	6.3845	5.7403
20	E	29.2249	26.8227	24.5815	22.4917	20.5444	18.7310
	K	23.1944	21.2878	19.5091	17.8506	16.3051	14.8658
	G	11.3275	10.3964	9.5277	8.7177	7.9629	7.2601
30	E	33.5943	31.0792	28.7149	26.4933	24.4069	22.4485
	K	26.6621	24.6661	22.7896	21.0264	19.3705	17.8163
	G	13.0210	12.0462	11.1298	10.2687	9.4600	8.7010
40	E	37.8195	35.1988	32.7202	30.3771	28.1629	26.0716
	K	30.0154	27.9355	25.9684	24.1088	22.3515	20.6918
	G	14.6587	13.6429	12.6823	11.7741	10.9159	10.1053
50	E	41.9328	39.2189	36.6390	34.1875	31.8589	29.6479
	K	33.2800	31.1261	29.0786	27.1330	25.2849	23.5300
	G	16.2530	15.2011	14.2012	13.2510	12.3484	11.4914
60	E	45.9562	43.1631	40.4962	37.9506	35.5215	33.2044
	K	36.4732	34.2564	32.1398	30.1195	28.1917	26.3527
	G	17.8125	16.7299	15.6962	14.7095	13.7680	12.8699
70	E	49.9051	47.0477	44.3086	41.6835	39.1684	36.7594
	K	39.6072	37.3395	35.1656	33.0822	31.0861	29.1741
	G	19.3431	18.2356	17.1739	16.1564	15.1816	14.2478

Table 11. The dependence of elastic constants C_{11} , C_{12} , C_{44} (10^{10} Pa) on pressure and concentration of interstitial atoms for BCC-FeSi at $T = 300$ K calculated by the SMM

P (GPa)	csi(%)	0	1	2	3	4	5
10	C_{11}	32.3141	29.2995	26.5171	23.9508	21.5856	19.4076
	C_{12}	13.1987	11.9674	10.8309	9.7827	8.8167	7.9271
	C_{44}	9.5577	8.6660	7.8431	7.0840	6.3845	5.7403
20	C_{11}	38.2977	35.1497	32.2127	29.4742	26.9223	24.5459
	C_{12}	15.6427	14.3569	13.1573	12.0388	10.9964	10.0258
	C_{44}	11.3275	10.3964	9.5277	8.7177	7.9629	7.2601
30	C_{11}	44.0235	40.7277	37.6293	34.7180	31.9839	29.4176
	C_{12}	17.9814	16.6352	15.3697	14.1806	13.0638	12.0156
	C_{44}	13.0210	12.0462	11.12979	10.2687	9.4600	8.7010
40	C_{11}	49.5604	46.1261	42.8781	39.8076	36.9060	34.1655
	C_{12}	20.2430	18.8402	17.5136	16.2594	15.0743	13.9549
	C_{44}	14.6587	13.6429	12.6823	11.7741	10.9159	10.1053
50	C_{11}	54.9508	51.3942	48.0135	44.8010	41.74941	38.8519
	C_{12}	22.4447	20.9920	19.6111	18.2990	17.0526	15.8691
	C_{44}	16.2530	15.2011	14.2012	13.2510	12.3484	11.4914
60	C_{11}	60.2232	56.5630	53.0681	49.7322	46.5490	43.5126
	C_{12}	24.5982	23.1032	21.6757	20.3132	19.0130	17.7728
	C_{44}	17.8125	16.7299	15.6962	14.7095	13.7680	12.8699
70	C_{11}	65.3980	61.6536	58.0641	54.6241	51.3281	48.1712
	C_{12}	26.7118	25.1824	23.7163	22.3112	20.9650	19.6756
	C_{44}	19.3431	18.2356	17.1739	16.1564	15.1816	14.2478

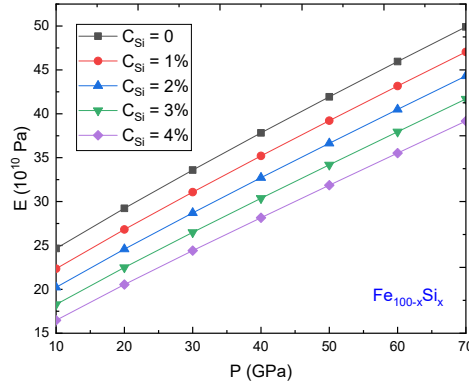


Figure 7. $E(P)(10^{10} \text{ Pa})$ for BCC-FeSi at $T = 300 \text{ K}$ calculated by the SMM

According to Tables 8-10 and Figures 7-9 for FeSi at $T = 300 \text{ K}$ and in the same pressure when the concentration of interstitial atoms increases, the mean nearest neighbor distance and quantities $E, G, K, C_{11}, C_{12}, C_{44}$ increase. For FeSi at $T = 300 \text{ K}$ and in the same concentration of interstitial atoms when pressure increases, the mean nearest neighbor distance, and quantities $E, G, K, C_{11}, C_{12}, C_{44}$ decrease. That agrees with the experimental law.

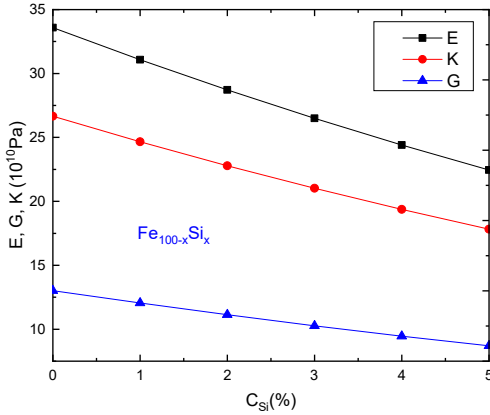


Figure 8. $E, K, G(c_{Si})(10^{10} \text{ Pa})$ for BCC-FeSi at $P = 30 \text{ GPa}, T = 300 \text{ K}$ calculated by the SMM

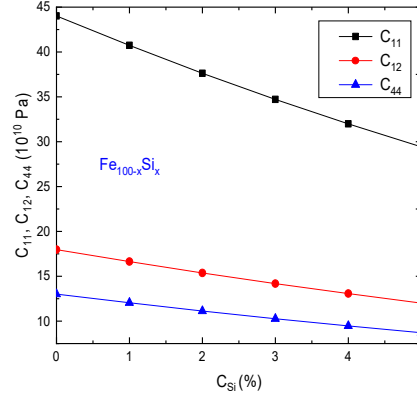


Figure 9. $C_{11}, C_{12}, C_{44}(c_{Si})(10^{10} \text{ Pa})$ for BCC-FeSi at $P = 30 \text{ GPa}, T = 300 \text{ K}$ calculated by the SMM

In our previous paper [28], we used the Mie-Lennard-Jones potential for interactions Fe-Fe and Si-Si where potential parameters were in [11] and the Mie-Lennard-Jones potential for interaction Fe-Si where

$$D_{\text{Fe-Si}} = \sqrt{D_{\text{Fe-Fe}} \cdot D_{\text{Si-Si}}}, r_{0\text{Fe-Si}} = \frac{1}{2}(r_{0\text{Fe-Fe}} + r_{0\text{Si-Si}}) \quad (31)$$

and parameters m and n were fitted with the experimental data of Young modulus in Ref. [29]. In this paper, when we use the model atomic potential for interaction Fe-Si, we do not

apply the above-mentioned process of fitting. However, both ways of using potential give the same law of elastic deformation in respect to temperature, pressure, and concentration of interstitial atoms.

3. Conclusions

From the obtained theoretical results and using the combination of the Mie-Lennard-Jones potential and the model atomic potential, we calculated numerically characteristic quantities for elastic deformation of BCC-FeSi. We obtain the values of elastic moduli, elastic constants, and compare the calculated results with experiments and other calculations. Some of our calculated results are in good agreement with available experiments and other calculated results predict experiments in the future.

REFERENCES

- [1] N.Q.Hoc, B.D.Tinh, L.D.Tuan and N.D.Hien, 2016. Elastic deformation of binary and ternary interstitial alloys with FCC structure and zero pressure: Dependence on temperature, concentration of substitution atoms and concentration of interstitial atoms. *Journal of Science of HNUE*, Vol. 61, No. 7, pp. 47-57.
- [2] N.Q. Hoc and N.D. Hien, 2017. Study on elastic deformation of interstitial alloy AB with BCC structure under pressure. *Proc. of the 10th National Conference on Solid State Physics and Material Science (SPMS)*, Hue city, 19-21 October, p. 911-914.
- [3] N. Q. Hoc, N.T. Hoa and N.D. Hien, 2017. Study on elastic deformation of substitution alloy AB with interstitial atom C and BCC structure under pressure. *Scientific Journal of Hanoi Metropolitan University*, No. 20, pp. 55-66.
- [4] N.Q. Hoc and N.D. Hien, 2018. Study on elastic deformation of substitutional alloy AB with interstitial atom C and FCC structure under pressure. *HNUE Journal of Science*. Vol. 63, Issue 3, pp. 23-33 (in Vietnamese).
- [5] Hoc Q. Nguyen and Hien D. Nguyen, 2018. Study on elastic deformation of substitution alloy AB with interstitial atom C and BCC structure under pressure. *42nd Vietnam National Conference on Theoretical Physics (NCTP-42)*, IOP Conf. Series: Journal of Physics: Conf. Series, Vol. 1034, 012005.
- [6] Hoc N.Q., Tinh B.D. and Hien N.D., 2018. Elastic moduli and elastic constants of interstitial alloy AuCuSi with FCC structure under pressure. *High Temperature Materials and Processes* <https://doi.org/10.1515/htmp-2018-0027>.
- [7] N.Q. Hoc, N.T. Hoa, N.D. Hien and D.Q. Thang, 2018. Study on nonlinear deformation of binary interstitial alloy with BCC structure under pressure. *HNUE Journal of Science*, Vol. 63, Issue 6, pp. 57-65.
- [8] N.Q. Hoc, N.D. Hien and D.Q. Thang, 2018. Elastic deformation of alloy AuSi with BCC structure under pressure. *HNUE Journal of Science*, Vol. 63, Issue 6, pp. 74-83.
- [9] Tinh B.D., Hoc N.Q., Vinh D.Q., Cuong T.D. and Hien N.D., 2018. Thermodynamic and elastic properties of interstitial alloy FeC with BCC structure at zero pressure. *Advances in Materials Science and Engineering*, Vol. 2018, Article ID 5251741, 8 pages.
- [10] Hoc N.Q., Cuong T.D. and Hien N.D., 2019. Study on elastic deformation of interstitial alloy FeC with BCC structure under pressure. *Proc. the ACCMS-Theme Meeting on "Multiscale Modelling of Materials for Sustainable Development"*, 7th - 9th September, 2018, VNU, Hanoi, *VNU Journal of Sciences*, Vol. 35, Issue 1, pp. 1-12.

- [11] Magomedov M. N., 1987. Calculation of temperature Debye and parameter Gruneisen. *Zh. Fiz. Khim.*, Vol. 61, No.4, pp.1003-1009 (in Russian).
- [12] Cleveland J. H., 1951, *Atom movements*, Ed. Hollomon, p. 260.
- [13] Lau T. T., Först C. J., Lin X., Gale J. D., Yip S. and Van Vliet K. J., 2007. Many-body potential for point defect clusters in Fe-C alloys. *Physical Review Letters*, Vol.98, No.21, p.215501.
- [14] Brosh E., Makov G. and Shneck R.Z., 2007. Application of CALPHAD to high pressure. *Calphad*, Vol.31, No.2, pp.173-185.
- [15] Georg R.B., Halliday A.N., Schauble E.A. and Reynolds B.C., 2007. Silicon in the Earth's core. *Nature*, Vol. 447, pp. 1102-1107.
- [16] N.Q. Hoc, D.Q. Vinh, B.D. Tinh, N.L. Phuong, T.T.C. Loan, T.T. Hue and D.T.T. Thuy, 2015. Thermodynamic properties of binary interstitial alloys with BCC structure: Dependence on temperature and concentration of interstitial atoms. *HNUE Journal of Science*, Vol. 60, Issue 7, pp.146-155.
- [17] Hoc N.Q. and Viet L.H., 2017. Influence of vacancy on thermodynamic properties of interstitial alloy FeSi with BCC structure under pressure. *Proc. of the 10th National Conference on Solid State Physics and Material Science (SPMS)*, Hue city, 19-21 October, 2017, pp.907-910.
- [18] Hoc N.Q., Hoa N.T., Cuong T.D. and Thang D.Q., 2019. On the melting of interstitial alloys FeH, FeSi and FeC with a body-centered cubic structure under pressure. *Proc. the ACCMS-Theme Meeting on "Multiscale Modelling of Materials for Sustainable Development"*, 7th-9th September, 2018, VNU, Hanoi, *Vietnam Journal of Science, Technology and Engineering*, Vol. 61, No. 2, pp. 17-22.
- [19] Paidá V., 1972. Elastic properties and model atomic interactions in Fe-Si alloys. *Czechoslovak Journal of Physics B*, Vol.22, pp.938-951.
- [20] V.V.Hung, 2009, *Statistical moment method in studying elastic and thermodynamic properties of crystals*. University of Education Publishing House, Hanoi (in Vietnamese).
- [21] Magomedov M. N., 2011. Activated-process parameters for diamond, silicon and germanium crystals. *Russian Microelectronics*, Vol.40, No.8, pp. 567-573.
- [22] Kępczak N., Pawłowski W. and Kaczmarek L., 2015. Cast iron and mineral cast applied for machine tool bed – dynamic behavior analysis. *Archives of Metallurgy and Materials*, Vol.60, No.2, pp.1024-1029.
- [23] Basinski Z. S., Hume-Rothery W. and Sutton A. L., 1955. The lattice expansion of iron. *Proceedings of the Royal Society of London A*, Vol. 229, No.1179, pp. 459-467.
- [24] Clendenen R. L. and Drickamer H. G., 1964. The effect of pressure on the volume and lattice parameters of ruthenium and iron. *Journal of Physics and Chemistry of Solids*, Vol.25, No.8, pp.865-868.
- [25] Anderson O. L. and Lee P. A., 1995. *Equations of state of solids for geophysics and ceramic science*, No. 31, Oxford University Press on Demand.
- [26] Sha X. and Cohen R. E., 2006. First-principles thermoelasticity of bcc iron under pressure. *Physical Review B* Vol. 74, No.21, p. 214111.
- [27] Adams J. J., Agosta D. S., Leisure R. G. and Ledbetter H., 2006. Elastic constants of monocrystal iron from 3 to 500K. *Journal of Applied Physics*, Vol. 100, No.11, p.113530.
- [28] Hoc N.Q., Hoa N.T. and Hien N.D., 2019. Nonlinear deformation of interstitial alloy FeSi with BCC structure. *Report at the 11th National Conference on Solid Physics and Materials Science (SPMS 2019)*, Qui Nhon city, 2nd - 4th November.
- [29] Fiorillo F., Bertotti G., Appino C. and Pasquale M., 1999. *Soft Magnetic Materials*. Wiley Encyclopedia of Electrical and Electronics Engineering.